

Metasurface Sensing Difference in Waveforms at the Same Frequency with Reduced Power Level

Mizuki Tanikawa¹, Daiju Ushikoshi¹, Kosei Asano¹, Kenichiro Sanji², Masakazu Ikeda², Daisuke Anzai¹, and Hiroki Wakatsuchi^{1,3,*}

¹Department of Electrical and Mechanical Engineering, Graduate School of Engineering, Nagoya Institute of Technology, Nagoya, Aichi, 466-8555, Japan

²Research Department 23, Research & Development Department 2, SOKEN, INC., Nisshin, Aichi, 470-0111, Japan

³Precursory Research for Embryonic Science and Technology (PRESTO), Japan Science and Technology Agency (JST), Kawaguchi, Saitama, 332-0012, Japan

*wakatsuchi.hiroki@nitech.ac.jp

ABSTRACT

We numerically demonstrate a new type of waveform-selective metasurface that senses the difference in incoming waveforms or pulse widths at the same frequency. Importantly, the proposed structure contains precise rectifier circuits that, compared to ordinary schottky diodes used within old types of structures, rectify induced electric charges at a markedly reduced input power level depending on several design parameters but mostly on the gain of operational amplifiers. As a result, a waveform-selective absorbing mechanism related to this turn-on voltage appears even with a limited signal strength that is comparable to realistic wireless signal levels. In addition, the proposed structure exhibits a noticeably wide dynamic range from -30 to 6 dBm, compared to a conventional structure that operated only around 0 dBm. Thus, our study opens up the door to apply the concept of waveform selectivity to a more practical field of wireless communications to control different small signals at the same frequency.

In modern society our daily life benefits from various wireless communication devices including smartphones, Bluetooth/WiFi/IoT (Internet of Things) devices, broadcasting antennas for television/radio, radar systems for weather forecasting and GPS (global positioning system) satellites. On one hand, there is strong demand on developing more advanced wireless communication technologies or services to further enhance the quality of our life. On the other hand, this continuous development escalates a potential risk for communication devices to be exposed to other wireless signals unnecessarily, leading to unexpected electromagnetic interference issues¹. These issues are especially serious in the ISM (industrial, scientific and medical) bands, which are standardized to be readily used without strict licence procedures. For instance, 13.5 MHz and 2.4 GHz are well known to be used for RFID and WiFi technologies, respectively.

A conventional solution to these interference issues is deploying absorbent materials that effectively dissipate the energy of an incoming wave at a designed frequency (or band) and thus suppress the magnitude of the scattering wave to an acceptable level². Although a traditional type of absorber was relatively bulky to the wavelength of an incident wave³, absorbers composed of artificially engineered periodic structures, or the so-called metamaterials/metasurfaces⁴⁻¹¹, can be designed in a limited space with subwavelength thicknesses and light weights, thereby enhancing their applicability to various situations and successfully mitigating electromagnetic interference issues¹²⁻²⁰. However, electromagnetic interference becomes more complicated once the spectrum of a wireless communication signal overlaps that of other signal/noise. This is because if the incoming spectrum is fixed, ordinary materials similarly respond to different waves and thus are incapable of distinguishing one signal from another. As opposed to these conventional materials, however, circuit-based metasurface absorbers were recently demonstrated to be capable of absorbing a particular type of incoming wave even at the same frequency by sensing its waveform or pulse width²¹⁻²⁶. Such a waveform-selective mechanism was thus expected to give us an additional degree of freedom to control electromagnetic waves/signals and solve electromagnetic interference issues occurring at the same frequency. A remaining issue here, however, is that due to the turn-on voltage of the diodes integrated with the structures, any of waveform-selective metasurfaces reported to date required an extremely large input power level, compared to the strength of most wireless communication signals²⁷. Hence, this issue hindered fully exploiting the concept of waveform selectivity in realistic wireless communication environment.

For this reason, we propose a new type of waveform-selective metasurface that is numerically demonstrated to operate at a low power level but still selectively absorbs a particular waveform at the same frequency. This is achieved by replacing

conventional diodes with precise rectifier circuits (PRCs)²⁸ that markedly lower turn-on voltage depending on the gain of operational amplifiers (op-amps) used.

Structure and waveform-selective mechanism

The waveform-selective metasurface demonstrated in this numerical study consisted of metallic patches ($1,600 \times 1,600 \text{ mm}^2$), a dielectric substrate (Rogers3003, 300 mm thickness) and a ground plane (Fig. 1a). The periodicity of the structure was set to a large value (1,700 mm), although entire dimensions can be readily scaled down by introducing lumped capacitors between metallic patches to lower the resonant frequency even with a small periodicity. Additionally, each gap between conducting patches was connected by four diodes that worked as a diode bridge (Figs. 1b and c). Under these circumstances, the diode bridge converts the incoming spectrum to an infinite set of frequency components, although most of the energy appears at zero frequency as the waveform is fully rectified^{21,23,25}. Therefore, by connecting a capacitor to a resistor in parallel within the diode bridge (Figs. 1b and c)²¹, the energy of the incoming pulsed wave can be firstly stored within the structure and dissipated at the resistor before a next pulse comes in. However, this capacitor-based waveform-selective metasurface lowers its absorbing performance when the incoming waveform changes to long pulse or continuous wave (CW), because the capacitor used is fully charged up. Other types of waveform-selective metasurfaces are seen in our previous studies^{23,29}.

Simulation method

This structure was numerically tested by using a co-simulation method integrating an electromagnetic simulator with a circuit simulator (ANSYS Electronics Desktop R18.1.0)²¹. Compared to ordinary electromagnetic simulation methods^{30–32}, the co-simulation method significantly reduced a total simulation time at the expense of fully visualizing spatial electromagnetic field distribution³³, since eventually all of simulation results were obtained in circuit simulations (Fig. 1b). In the co-simulation method, a single periodic unit cell was modelled using periodic boundaries to effectively represent an infinite array of periodic structure (see Fig. 1a). An incident wave was generated from a Floquet port deployed on the top of the entire analysis space. The frequency was changed from 20 to 50 MHz with the power level varied from -50 to 0 dBm. Unlike our past studies³⁴ where only “one” lumped port was used to model circuit components (i.e., a diode bridge, resistor and capacitor) between two conducting patches and to effectively assume one of the conductor edges as a ground, the model of Fig. 1a had “two” lumped ports between a ground plane and patches (see also Fig. 1b). This is because the new rectifying circuits proposed later in this study contained additional grounds that could not be electrically connected to the above-mentioned ground.

Table 1. Design parameters used for a periodic unit cell of the waveform-selective metasurface drawn in Fig. 1.

Variables	Values	Variables	Values
p	1,700 mm	C	100 nF
h	300 mm	R	100 k Ω
g	100 mm		

Precise rectifier circuit

Practically, commercial schottky diodes have turn-on voltage of a few hundred mV or so. For example, Fig. 2 shows the relationship between voltage and current, namely, I - V curve of a schottky diode (Broadcom, HSMS2860 but without parasitic junction capacitance C_{J0} and series resistance R_S for the sake of simplicity). By approximating this curve by a straight line at a sufficiently large voltage (e.g., 1 V) and reading its intersection with the horizontal axis (as marked by the black cross in Fig. 2), turn-on voltage V_{on} of the diode is estimated to be around 0.3 V.

In this study, V_{on} was decreased by alternatively using the PRC drawn in Fig. 3a²⁸. Basically, this circuit took the form of an inverse amplifier circuit and contained one ideal op-amp, four resistors and two diodes (the same model as Fig. 2). In general, output voltage V_{out} of this entire circuit is associated with input voltage V_{in} as

$$V_{out} = \begin{cases} -R_2(V_{in} - V_{on})/R_1 & (V_{in} > V_{on}) \\ 0 & (V_{in} < V_{on}), \end{cases} \quad (1)$$

where R_1 and R_2 are resistances used in the circuit (see Fig. 3a). Ideally, V_{on} is

$$V_{on} = V_0/A, \quad (2)$$

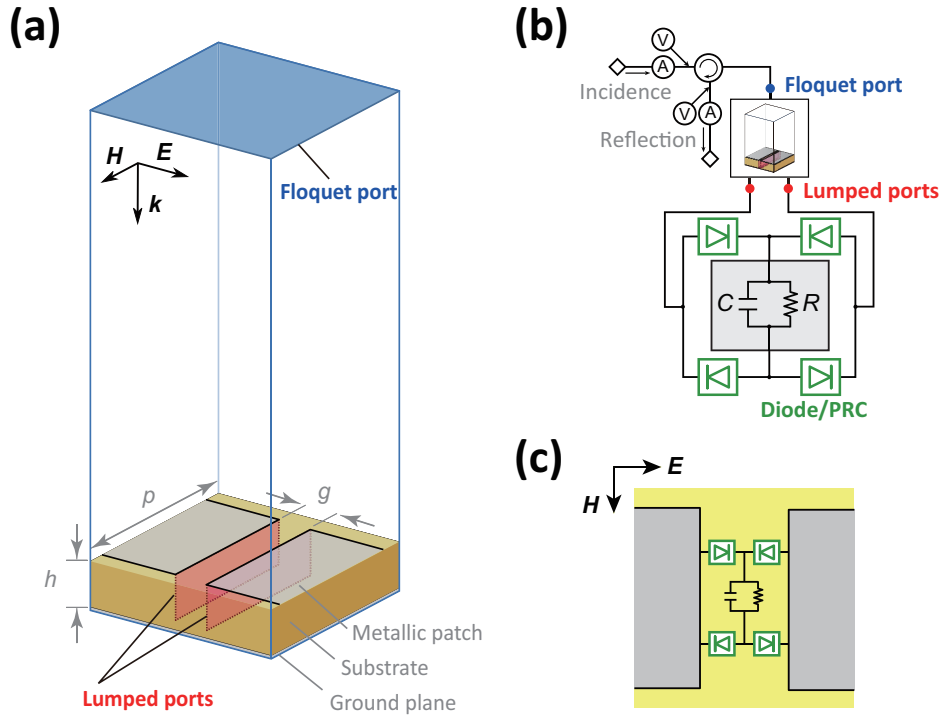


Figure 1. (a) Electromagnetic model, (b) circuit schematic diagram and (c) equivalent electromagnetic structure. Additional circuit components deployed inside a diode bridge. Design parameters are given in Table 1, and PRC is seen in Fig. 3a.

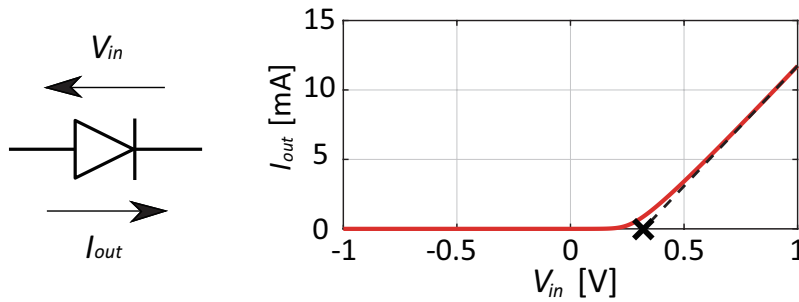


Figure 2. I - V characteristics of schottky diode used in this study (Broadcom, HSMS2860). The black cross represents its turn-on voltage.

where V_0 is the turn-on voltage of the diodes included in the PRC, and A represents the gain of the op-amp. Hence, V_{on} is inversely proportional to A .

However, this turn-on voltage is also influenced by resistances as demonstrated in Fig. 3b, where R_1 , R_2 and $R_3/2$ are determined by R_0 , while R_4 is fixed at 50Ω . For instance, with small R_0 the current flowing into diode D_2 of Fig. 3 is almost independent of R_0 (Fig. 4a). However, the current at R_2 varies as the resistor is effectively shorted (Fig. 4b). Since these two currents determine the output current based on Kirchhoff's current law, the turn-on voltage increases by using a small resistance value such as 10Ω compared to $1 \text{ k}\Omega$ (Fig. 4c). Note that these current curves are changed by the gain of the op-amp so that the turn-on voltage is still inversely proportional to A (Fig. 3b).

With extremely large R_0 such as $R_0 = 1 \text{ M}\Omega$, the turn-on voltage increases again. Although an ideal diode does not permit electric charges to enter from its anode to cathode, a more realistic diode has saturation current, which varies the amount of the current reversely coming into D_1 of Fig. 3a as drawn in Fig. 5a, where saturation current I_S is set to two different values. When I_S saturates, R_2 starts increasing its current, which relates to the output current as well (Fig. 5b). Importantly, the larger R_0 , the larger V_{on} becomes (cf. Fig. 5c). Also, these characteristics are independent of the gain of the op-amp so that with large R_0 , V_{on} becomes not only larger but also independent of A (see around $R_0 = 1 \text{ M}\Omega$ in Fig. 3b).

Based on these results, circuit parameters need to be properly designed, otherwise the operating power level of a waveform-

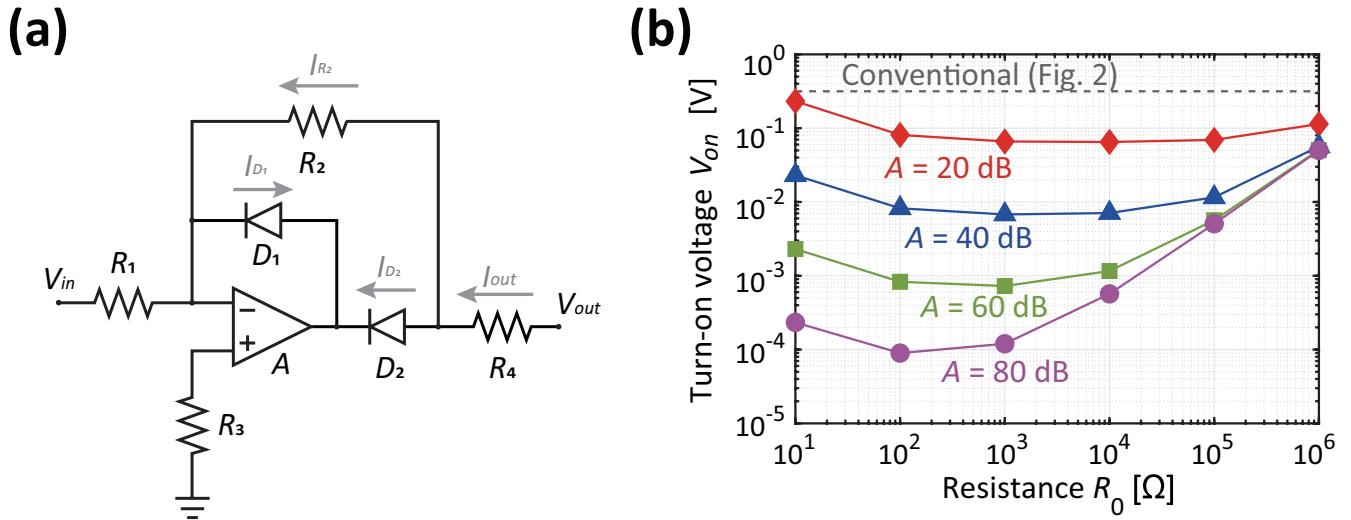


Figure 3. (a) Proposed PRC and (b) its turn-on voltage with resistances set to $R_1 = R_2 = R_3/2 = R_0$ and $R_4 = 50 \Omega$. For the top two PRCs of Figs. 1b and c, the orientations of D_1 and D_2 were changed, while those for the bottom two remained the same as the ones shown above.

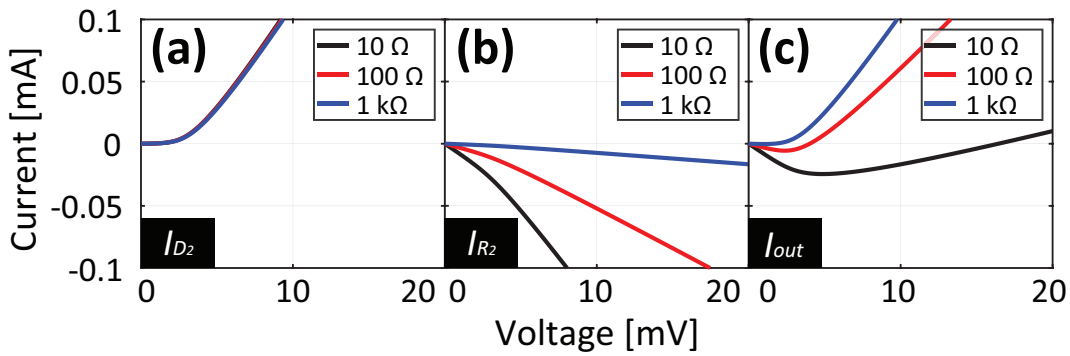


Figure 4. Currents at (a) D_2 , (b) R_2 and (c) R_4 shown in Fig. 3 with small R_0 .

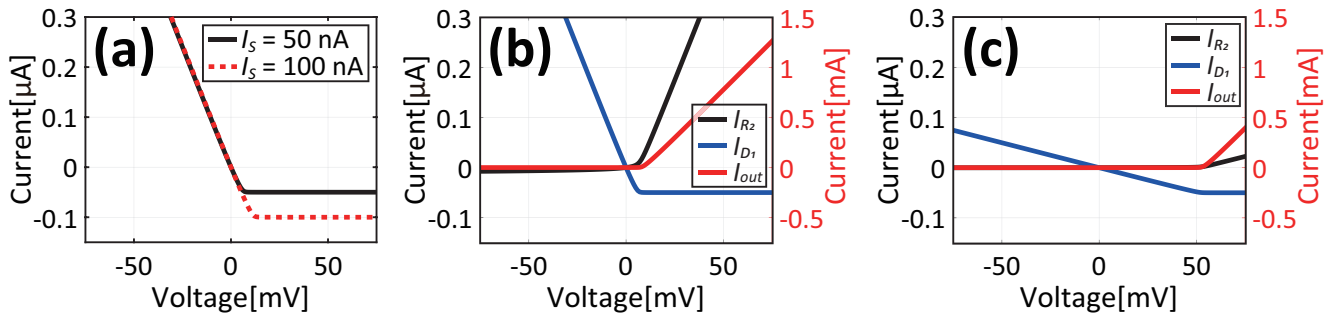


Figure 5. (a) Current at D_1 shown in Fig. 3 with various saturation current values. Currents at D_1 , R_2 and R_4 with (b) $R_0 = 100 \text{ k}\Omega$ and (c) $R_0 = 1 \text{ M}\Omega$.

selective metasurface would not be improved. In the following part of this study, R_1 , R_2 , R_3 and R_4 are, respectively, set to $10 \text{ k}\Omega$, $10 \text{ k}\Omega$, $5 \text{ k}\Omega$ and 50Ω as default values, while A is basically fixed at 40 dB (Table 2).

In addition, the orientations of D_1 and D_2 are changed for the top two PRCs of Fig. 1b, while those for the bottom two remain the same as the ones shown in Fig. 3a. This is because electric charges coming into an op-amp change their sign. Therefore, unless the diodes of the next PRC are aligned for another direction, the electric charges are not allowed to reach an

Table 2. Default values used for precise rectifier circuits.

Variables	Values	Variables	Values
A	40 dB	R_3	5 k Ω
R_1, R_2	10 k Ω	R_4	50 Ω

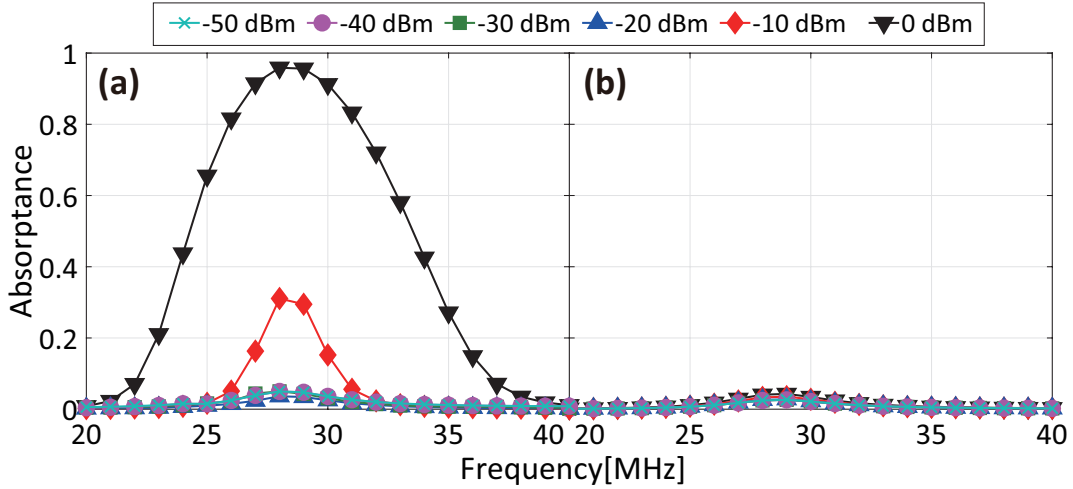


Figure 6. Absorbance of a conventional capacitor-based waveform-selective metasurface using schottky diodes for (a) 5- μ s short pulse and (b) CW.

adjacent conducting patch (also, their sign is not restored).

Simulated absorbing performance

To evaluate improvement on the operating power of the proposed structure, we firstly simulated a capacitor-based waveform-selective metasurface using conventional commercial schottky diodes as shown in Fig. 6. This figure demonstrates that the structure was incapable of strongly absorbing any waveform within the power range between -50 and -20 dBm. Then the capacitor-based waveform-selective metasurface enhanced its absorbance for a short pulse by increasing the power level to 0 dBm, which, however, exceeds the strength of ordinary wireless communication signals²⁷. We also note that this absorbing mechanism was consistent with the theory mentioned above as well as with previous studies despite the difference in operating frequencies³⁴. Another point here is that the difference in absorbances of a short pulse and a CW is larger than that in our previous reports. This is because our structure used relatively a large time constant, which increased the difference between its response to a short pulse and that to a CW and thus contributed to enhancing the waveform-selective performance.

Secondly, this structure was simulated using the proposed PRCs instead of the conventional diodes. As plotted in Fig. 7, a waveform-selective absorbing mechanism appeared even if the input power was set to merely -40 dBm. The difference between the absorbance for a short pulse and that for a CW was maximized within the power range between -30 and -10 dBm. For instance, the capacitor-based waveform-selective metasurface absorbed 97.3 % of a short pulse and 38.5 % of a CW at the same frequency of 29 MHz. We also noticed that the gap between the pulse absorbance and the CW absorbance was reduced to about 60 % (with -20 dBm), compared to approximately 90 % difference seen in Fig. 6 (with 0 dBm). This is probably because electric charges rectified by the PRCs were dissipated by not only resistors but also the PRCs that contained additional resistors.

Regarding this point, Fig. 8 shows how R_0 related to the absorbances of the capacitor-based waveform-selective metasurface using the PRCs. As seen in this figure, where the input frequency and power were fixed at 29 MHz and -30 dBm, respectively, the CW absorbance was found to be suppressed by increasing R_0 from 10 k Ω . At the same time, however, this led to lowering the short-pulse absorbance as well. This is because entirely the turn-on voltage of the PRCs was increased as explained in Figs. 3 and 5. Therefore, the difference in the absorbances needs to be increased by properly designing R_0 . In addition, this absorbance gap may be enlarged by independently adjusting the resistive components of the PRCs, although

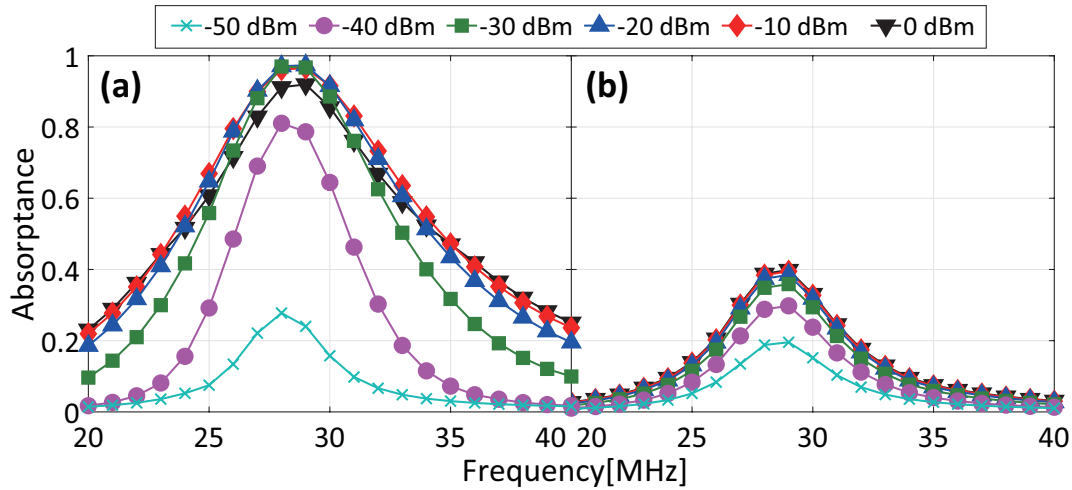


Figure 7. Absorbance of a proposed capacitor-based waveform-selective metasurface using PRCs for (a) 5- μ s short pulse and (b) CW.

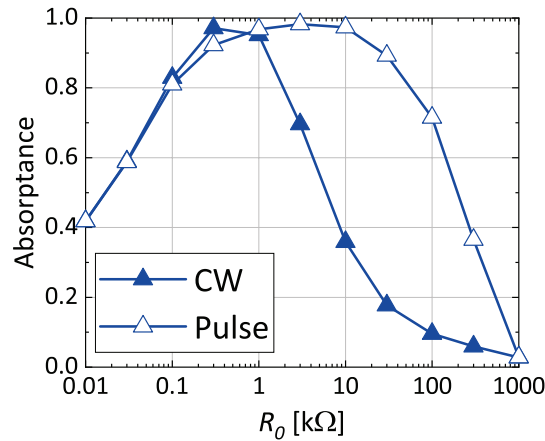


Figure 8. R_0 dependence of absorbance of capacitor-based waveform-selective metasurface using PRCs. The frequency and input power were fixed at 29 MHz and -30 dBm, respectively.

our study set R_1 , R_2 and R_3 to be $R_1 = R_2 = R_3/2$ for the sake of simplicity. Moreover, Fig. 8 also shows that the CW absorbance approached the short-pulse absorbance by decreasing R_0 from 10 k Ω . This trend is also explained by the turn-on voltage characteristics of the PRCs (refer to Figs. 3 and 4 again). We noticed that the short-pulse absorbance became slightly smaller than the CW absorbance for $R_0 < 1$ k Ω . This minor gap is possibly due to the small difference between the frequency spectra of both waveforms (i.e., the short pulse contained the oscillating frequency component mostly but also other minor components).

The improvement on the operating power level of the proposed structure is more clearly seen in Fig. 9a, which plots the absorbances of the two structures as a function of input power (with frequency fixed at 29 MHz). According to this result, the conventional structure required 0 dBm input power to achieve almost 100 % absorbance. However, our proposed structure reduced this power level to -30 dBm or so. Note that this improvement (about 30 dB) almost matched the gain of the op-amp, which was set to 40 dB in this study, although a minor discrepancy appeared as the turn-on voltage of PRC was slightly worse than expected from the gain (refer to Fig. 3). However, our results still support that waveform-selective metasurfaces can operate at a markedly reduced power level by lowering turn-on voltage of rectifier circuits, which was achieved through use of PRCs. Additionally, Fig. 9b shows the short-pulse absorbance of the capacitor-based waveform-selective metasurface using PRCs with various gain values. This figure clearly demonstrates that the turn-on voltage is improved proportionally to gain A .

Moreover, Fig. 9a indicates that our new structure not only lowered its operating power level but also improved a dynamic range of waveform-selective absorbing mechanism. Specifically, our structure showed almost 100 % absorbance between

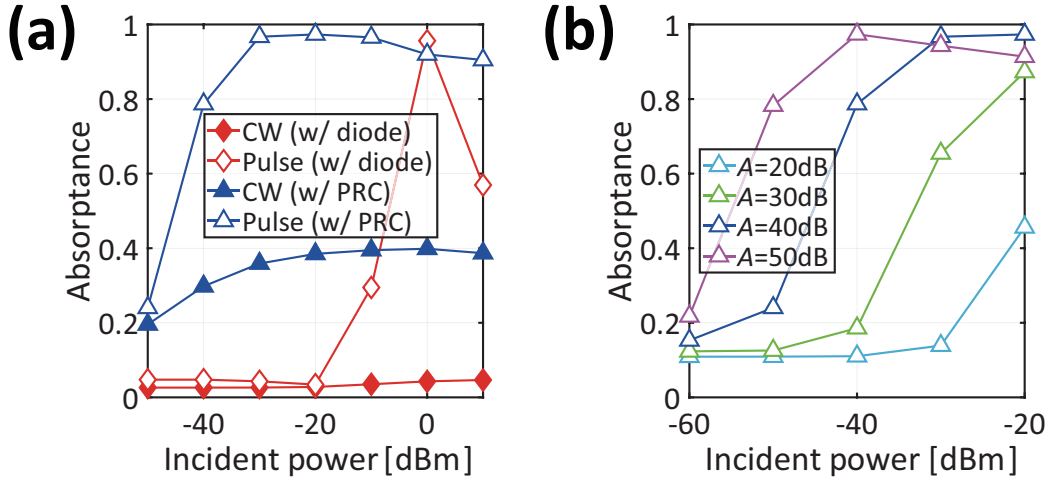


Figure 9. Power dependence of absorptance of (a) capacitor-based waveform-selective metasurfaces using either schottky diodes or PRCs with $A = 40$ dB and frequency fixed at 29 MHz. (b) Power dependence of pulse absorptance of the proposed capacitor-based waveform-selective metasurface using PRCs with various gains.

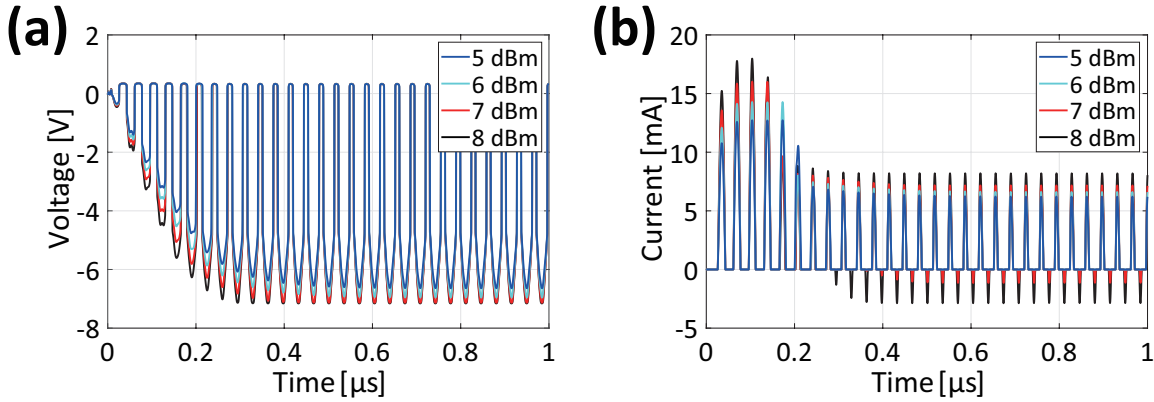


Figure 10. (a) Voltage and (b) current of D_2 used as the top two PRCs in Figs. 1b and c.

-30 dBm and -10 dBm, which was limited to only around 0 dBm in the conventional structure (compare the open triangles of Fig. 9a to the open rhombuses). In the conventional structure, basically the dynamic range is limited by the turn-on voltage of diodes as well as their break-down voltage. In our proposed structure, the diodes included in PRCs were found to operate for a wide range of input power level, as op-amps adjusted the amount of current to come into anodes of diodes. In the case of Fig. 3a, for example, the op-amp amplified the input voltage only to turn on D_2 so that the voltage across D_1 did not reach its break-down voltage. In some cases, however, diodes were found to reach their break-down voltage as seen in Fig. 10, which plots the voltage and current of diode D_2 whose cathodes were oriented to the output (i.e., the same configuration as the one used for the top two PRCs of Fig. 1b). This figure shows that with an input power larger than 6 dBm the voltage across D_2 became -7 V, which was its break-down voltage (Fig. 10a). As a result, its current flowed both forwardly and reversely (Fig. 10b). Nonetheless, the use of these new rectifying circuits led to a broader dynamic range from -30 dBm to 6 dBm than the one seen in the conventional structure.

Discussion

The improvement on the operating power level relates not only to the gain of op-amps and the resistive component of PRCs but also to other factors including frequency, as practically op-amps have frequency-dependent gain and thus more strongly/weakly amplify incoming electric charges depending on frequency. Although our study used PRCs, conventional schottky diodes may be replaced by other rectifier circuits, as long as induced electric charges are properly controlled to enter the internal circuit components. In particular, biased transistors can be alternatively used as amplifier circuit elements instead of op-

amps. Many MOSFETs can work at a GHz range including 2.4 GHz (i.e., one of the ISM bands). For a higher frequency such as the millimetre wave band, the op-amps used in our study need to be replaced by more advanced amplifier circuit components (e.g., Microsemi, MMA025AA). In this case, potentially waveform selectivity can be achieved in the millimetre-wave band, although possibly more improvement/modification is required for the entire rectifier circuit design. Our waveform-selective metasurface was designed to operate around 30 MHz, where many existing commercial op-amps are expected to work (e.g., Texas Instruments provides the op-amps (OPA858) that have a gain larger than 40 dB in this frequency range). Although this study only provided numerical simulations, we emphasize that still the concept of our structure needs to be fully validated by experimental results. However, we also note that measurement results of many circuit-based metasurfaces containing op-amps have been so far reported in the MHz band. For instance, recently studied non-Foster-loaded metasurfaces have been experimentally validated in the MHz band³⁵. The maximum frequency to apply the concept of the PRC-based waveform-selective metasurface depends on what PRCs or op-amps are used, which is potentially more improved by using latest semiconductor technologies but was outside the scope of this study as an important point here was that the operating power level of waveform-selective metasurface can be improved by lowering the turn-on voltage of rectifier circuits used. Additionally, we note again that introducing lumped circuit elements (e.g., lumped capacitors) to the gap between conducting patches leads to readily lowering the operating frequency³⁴, which implies that our structure maintains the same operating frequency with a smaller periodicity. The only reason to adopt large physical dimensions in this study lies in avoiding a complexity in the structure and clarifying its underlying mechanism in a simple manner.

As a final remark, to theoretically predict a receiver power in wireless communication systems, propagation models have been so far discussed, i.e., two-wave propagation and multipath propagation models²⁷. Based on a simple two-wave propagation model with a transmitting power set to 0 dBm, for instance, an antenna located within 10 metres or so receives a signal level larger than -30 dBm. This power level is satisfied by our proposed approach. Although there still remain some issues including experimental validation, our results therefore contribute to exploiting the concept of waveform selectivity not only in fundamental electromagnetic research field but also in a more practical field of wireless communications.

Conclusion

We have proposed a new type of waveform-selective metasurface composed of PRCs instead of conventional schottky diodes. Our simulation results demonstrated that with proper design parameters applied to integrated resistors, PRCs had turn-on voltage that was inversely proportional to the gain of op-amps and lower than that of conventional schottky diodes. By using these PRCs, waveform-selective metasurfaces successfully reduced operating power level to approximately a thousandth, which was still changeable depending on the gain of op-amps used. As a result, waveform-selective absorption was achieved at a power level of -30 dBm, which is the same level as general communication systems, for example, Wi-Fi systems^{27,36}. In addition, the proposed structure exhibited a markedly wide dynamic range from -30 to 6 dBm, compared to a conventional structure that operated only around 0 dBm. Hence, our study is expected to open up the door to exploit the concept of waveform selectivity not only in fundamental electromagnetic research field but also in a more practical field of wireless communications to control different small signals at the same frequency³⁷.

References

1. Christopoulos, C. *Principles and techniques of electromagnetics compatibility* (CRC Press Taylor & Francis Group, London, U.K., 2007), second edn.
2. Knott, E. *Radar cross section measurements* (SciTech Publishing, Raleigh, NC, 2006).
3. Salisbury, W. W. Absorbent body for electromagnetic waves (1952). US Patent 2,599,944.
4. Pendry, J. B., Holden, A. J., Stewart, W. J. & Youngs, I. Extremely low frequency plasmons in metallic mesostructures. *Phys. Rev. Lett.* **76**, 4773–4776 (1996).
5. Pendry, J. B., Holden, A. J., Robbins, D. J. & Stewart, W. J. Magnetism from conductors and enhanced nonlinear phenomena. *IEEE Trans. Microw. Theory Tech.* **47**, 2075–2084 (1999).
6. Smith, D. R., Padilla, W. J., Vier, D. C., Nemat-Nasser, S. C. & Schultz, S. Composite medium with simultaneously negative permeability and permittivity. *Phys. Rev. Lett.* **84**, 4184–4187 (2000).
7. Shelby, R. A., Smith, D. R. & Schultz, S. Experimental verification of a negative index of refraction. *Science* **292**, 77–79 (2001).
8. Sievenpiper, D., Zhang, L., Broas, R. F. J., Alexópolous, N. G. & Yablonovitch, E. High-impedance electromagnetic surfaces with a forbidden frequency band. *IEEE Trans. Microw. Theory Tech.* **47**, 2059–2074 (1999).
9. Chen, H. *et al.* Active terahertz metamaterial devices. *Nature* **444**, 597–600 (2006).

10. Fong, B. H., Colburn, J. S., Ottusch, J. J., Visher, J. L. & Sievenpiper, D. F. Scalar and tensor holographic artificial impedance surface. *IEEE Trans. Antennas Propag.* **58**, 3212–3221 (2010).
11. Yu, N. *et al.* Light propagation with phase discontinuities: generalized laws of reflection and refraction. *Science* **334**, 333–337 (2011).
12. Munk, B. A. *Frequency selective surfaces: theory and design* (A Wiley–Interscience Publication, New York, NY, 2000).
13. Watts, C. M., Liu, X. & Padilla, W. J. Metamaterial electromagnetic wave absorbers. *Adv. Mater.* **24** (2012).
14. Li, A., Luo, Z., Wakatsuchi, H., Kim, S. & Sievenpiper, D. F. Nonlinear, active, and tunable metasurfaces for advanced electromagnetics applications. *IEEE Access* **5**, 27439–27452 (2017).
15. Landy, N. I., Sajuyigbe, S., Mock, J. J., Smith, D. R. & Padilla, W. J. Perfect metamaterial absorber. *Phys. Rev. Lett.* **100**, 207402 (2008).
16. Tao, H. *et al.* A metamaterial absorber for the terahertz regime: design, fabrication and characterization. *Opt. Express* **16**, 7181–7188 (2008).
17. Kern, D. J. & Werner, D. H. A genetic algorithm approach to the design of ultra–thin electromagnetic bandgap absorbers. *Microw. Opt. Technol. Lett.* **38**, 61–64 (2003).
18. Wakatsuchi, H., Greedy, S., Christopoulos, C. & Paul, J. Customised broadband metamaterial absorbers for arbitrary polarisation. *Opt. Express* **18**, 22187–22198 (2010).
19. Wakatsuchi, H., Kim, S., Rushton, J. J. & Sievenpiper, D. F. Circuit-based nonlinear metasurface absorbers for high power surface currents. *Appl. Phys. Lett.* **102**, 214103 (2013).
20. Li, A. *et al.* High-power transistor-based tunable and switchable metasurface absorber. *IEEE Trans. Microw. Theory Tech.* **65**, 2810–2818 (2017).
21. Wakatsuchi, H., Kim, S., Rushton, J. J. & Sievenpiper, D. F. Waveform-dependent absorbing metasurfaces. *Phys. Rev. Lett.* **111**, 245501 (2013).
22. Eleftheriades, G. V. Electronics: Protecting the weak from the strong. *Nature* **505**, 490–491 (2014).
23. Wakatsuchi, H. *et al.* Waveform selectivity at the same frequency. *Sci. Rep.* **5**, 9639 (2015).
24. Vellucci, S., Toscano, A., Bilotti, F., Monti, A. & Barbuto, M. Towards waveform-selective cloaking devices exploiting circuit-loaded metasurfaces. In *2018 IEEE International Symposium on Antennas and Propagation & USNC/URSI National Radio Science Meeting*, 1861–1862 (IEEE, 2018).
25. Wakatsuchi, H., Long, J. & Sievenpiper, D. F. Waveform selective surfaces. *Adv. Funct. Mater.* **29**, 1806386 (2019).
26. Vellucci, S., Monti, A., Barbuto, M., Toscano, A. & Bilotti, F. Waveform-selective mantle cloaks for intelligent antennas. *IEEE Trans. Antennas Propag.* **68**, 1717–1725 (2019).
27. Goldsmith, A. *Wireless communications* (Cambridge University Press, Cambridge, U.K., 34, 2005).
28. Stout, D. F. & Kaufman, M. *Handbook of operational amplifier circuit design* (McGraw-Hill Inc., New York, NY, 1976).
29. Wakatsuchi, H. Time-domain filtering of metasurfaces. *Sci. Rep.* **5**, 16737 (2015).
30. Jin, J.-M. *The finite element method in electromagnetics* (John Wiley & Sons, Hoboken, NJ, 2015).
31. Taflove, A. & Hagness, S. C. *Computational electrodynamics: the finite-difference time-domain method* (Artech house, Boston, MA, 2005).
32. Christopoulos, C. *The transmission–line modeling method: TLM* (IEEE press/Oxford University Press, Piscataway, NJ/Oxford U.K., 1995).
33. Wakatsuchi, H., Anzai, D. & Smartt, C. Visualization of field distributions of waveform-selective metasurface. *IEEE Antennas Wirel. Propag. Lett.* **15**, 690–693 (2016).
34. Wakatsuchi, H. Waveform-selective metasurfaces with free-space wave pulses at the same frequency. *J. Appl. Phys.* **117**, 164904 (2015).
35. Mou, J. & Shen, Z. Design and experimental demonstration of non-Foster active absorber. *IEEE Trans. Antennas Propag.* **65**, 696–704 (2016).
36. Ieee802.11: Part11: Wireless lan medium access control (mac) and physical layer (phy) specifications (2016).
37. Ushikoshi, D. *et al.* Experimental demonstration of waveform-selective metasurface varying wireless communication characteristics at the same frequency band of 2.4 ghz. *Electron. Lett.* (2019).

Acknowledgements

This work was supported in part by Denso, SOKEN and the Support Center for Advanced Telecommunications Technology Research (SCAT).

Author contributions statement

H.W. designed the entire project. M.T. designed specific PRCs and performed numerical simulations. All the authors considered the results and contributed to writing up the manuscript.

Competing financial interests

The authors declare no competing interests.